ELSEVIER

Journal of Fluids and Structures 26 (2010) 236–252

JOURNAL OF FLUIDS AND STRUCTURES

www.elsevier.com/locate/jfs

Coupled free vibration analysis of a fluid-filled rectangular container with a sagged bottom membrane

F. Daneshmand*,[1], E. Ghavanloo

Mechanical Engineering Department, School of Engineering, Shiraz University, Shiraz 71348-51154, Iran

Received 23 December 2008; accepted 2 November 2009
Available online 25 January 2010

Abstract

In the present paper, two-dimensional coupled free vibrations of a fluid-filled rectangular container with a sagged bottom membrane are investigated. This system consists of two rigid walls and a membrane anchored along two rigid vertical walls. It is filled with incompressible and inviscid fluid. The membrane material is assumed to act like an inextensible material with no bending resistance. First, the nonlinear equilibrium equation is solved and the equilibrium shape of the membrane is obtained using an analytical formulation neglecting the membrane weight. The small vibrations about the equilibrium configuration are then investigated. Along the contact surface between the bottom membrane and the fluid, the compatibility requirement is applied for the fluid–structure interactions and the finite element method is used to calculate the natural frequencies and mode shapes of the fluid–membrane system. The vibration analysis of the coupled system is accomplished by using the displacement finite element for the membrane and the pressure fluid-finite element for the fluid domain. The variations of natural frequencies with the pressure head, the membrane length, the membrane weight and the distance between two rigid walls are examined. Moreover, the mode shapes of system are investigated.

Keywords: Fluid–structure interaction; Sagged membrane; Fluid–membrane system; Coupled free vibration; Natural frequency

1. Introduction

Various types of fluid–structure interaction problems can be found in engineering and applied sciences. The most important ones are vibration analysis of the hydraulic gates (Daneshmand et al., 2004), sloshing motion of fluid in a tank (Yuanjun et al., 2007), earthquake response of water-retaining structures, pipes conveying fluid and containers (Padoussis et al., 2008), wind or fluid-induced vibration of bridge girders and vibration of offshore structures (Liang and Tai, 2006; Tao et al., 2007). Predicting the coupled motions of the fluid and the structures is generally a difficult task, and in most practical problems it is not possible to obtain closed form analytical solutions for coupled systems. The analysis of the fluid-filled storage containers and rigid or flexible boxes has been of great interest to many structural engineers in recent years (Jeong, 2006; Karagiozis et al., 2005; Biswal et al., 2004; Bermudez et al., 1997). Several

*Corresponding author. Tel.: +98 711 6287508; fax: +98 711 6275028.
E-mail addresses: daneshmd@shirazu.ac.ir, farhang.daneshmand@mcgill.ca (F. Daneshmand)
[1]Currently, Visiting Professor, Department of Mechanical Engineering, McGill University, 817 Sherbrooke Street W., Montreal, Québec, Canada H3A 2K6.

0889-9746/$ - see front matter © 2009 Elsevier Ltd. All rights reserved.
doi:10.1016/j.jfluidstructs.2009.11.001

analytical, semi-analytical and numerical approaches have been proposed to obtain the natural frequencies of fluid-filled storage containers and the other rigid or flexible rectangular boxes.

Bermudez and Rodriguez (1994) calculated the natural frequencies of the fluid-filled squared cavity with flexible boundaries. They solved the interior elastoacoustic problem by a finite element method which does not present spurious or circulation modes for nonzero frequencies. Chiba (1994) studied the axisymmetric free vibration of a flexible bottom plate in a cylindrical tank supported on an elastic foundation. Wang and Bathe (1997) calculated the natural frequencies and mode shapes of the fluid-filled rigid box. A new theory has been investigated for the dynamics of cylindrical shell-tanks with a flexible bottom and ring stiffeners by Amabili et al. (1998). The natural frequencies of an elastic thin-plate placed into a rectangular hole and connected to the rigid bottom slab of a rectangular container filled with fluid having a free surface have been studied by Cheung and Zhou (2000). Linear hydroelastic free vibration analysis of a cylindrical container with rigid side-wall and membrane bottom has been studied by Chiba et al. (2002). They considered small amplitude coupled free vibrations of a liquid and a membrane; in their study, the static deformation of the bottom membrane is neglected because of small membrane deformation.

In spite of the extensive field experiments and research in the area of the fluid–structure interaction problems, there has been no attempt to tackle the problem described in the present paper. Most researches have concentrated too much on the calculation of the natural frequencies of the rigid or flexible storage container including the small deformation of flexible bottom. Also, the effect of static deformation of the flexible bottom has been ignored in many previous studies.

The aim of this study is to present a framework for investigating the dynamic behavior of a fluid-filled rectangular container with a sagged bottom membrane. It should be noted that the problem considered in this paper is actually different because the static deformation of the bottom membrane is really large, and so more attention should be paid on it. Some physical applications, such as membrane roofs and floating roofs in petroleum container may be mentioned for the present study. Moreover, the proposed approach for the static and dynamic analysis can be used for static and dynamic study of the geomembrane tubes and foundations of the emergency bridges (Ghavanloo and Daneshmand, 2009) and breakwaters (Phadke and Cheung, 2003).

In the present paper, the natural frequencies and mode shapes of the coupled system are obtained. This system can be modeled as a sagged membrane which is anchored along two rigid vertical walls. The fluid inside the container is assumed to be incompressible and inviscid. The length of the membrane is longer than the distance between two walls. An inextensible membrane with no bending resistance is considered here. Because of inextensibility assumption, the tangential strain is equal to zero. A two-dimensional (plane-strain) problem is treated in which the membrane is an infinite cylinder with generators parallel to the horizontal plane. In other words, the membrane itself is assumed to be long and straight and the changes in cross-sectional area along the membrane length are neglected. These two assumptions facilitate the use of a two-dimensional model. To determine the equilibrium configuration of the membrane, the specific weight of the membrane is assumed to be negligible with respect to the specific weight of the fluid.

In this analysis, the nonlinear differential equations are solved analytically and the equilibrium shape of the membrane is obtained. Then, the linear, two-dimensional coupled vibration of the fluid–membrane system about the equilibrium shape is investigated. The vibration analysis of the coupled system is accomplished by using the displacement finite element for the membrane and the pressure finite element for the fluid domain. The first six frequencies and mode shapes of the coupled system are determined for different conditions. The effects of the pressure head, the membrane length, the membrane weight and the distance between two rigid walls on the natural frequencies are elucidated. Moreover, we will propose an approximate relationship between the natural frequencies of the fluid–membrane system and the pressure head when the other parameters are fixed.

2. Problem statement

We consider the problem of determining the small amplitude motions of an inviscid and incompressible fluid contained in a rectangular container with a sagged bottom membrane. Let Ω_f and Γ_s be the domains occupied by the fluid and the membrane, respectively, as shown in Fig. 1. Let us denote by Γ_0 the free boundary of the fluid and by Γ_s the interface between the membrane and the fluid.

Our objective is to obtain the governing equations of the membrane under the influence of the fluid pressure. We begin formulating the governing equations by considering the membrane in the deformed state, and identify point particles distributed along the membrane by the deformed-state arc length S varying in the range $[0,L]$, where L is the length of the membrane. The origin O is considered at the left end of the membrane. The coordinates are $X(S,T)$ and $Y(S,T)$, and the angle of the tangent with the horizontal is $\psi(S,T)$, where T is time. The distance between two rigid walls

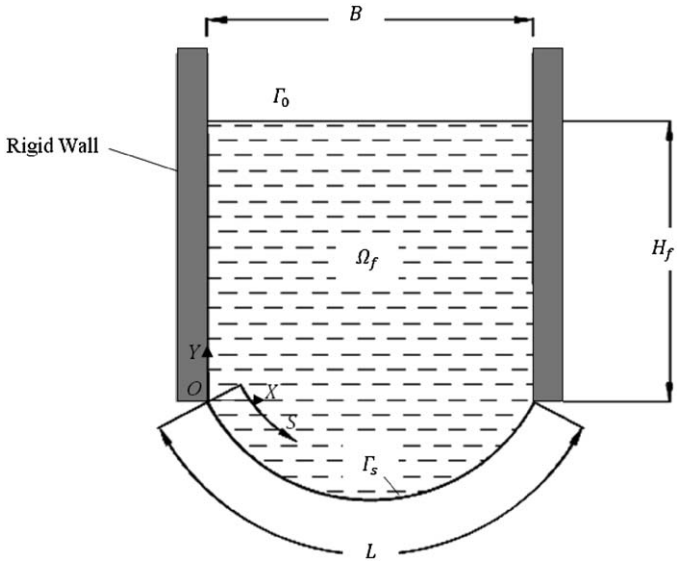

Fig. 1. Rectangular container with a sagged bottom membrane filled with an incompressible liquid.

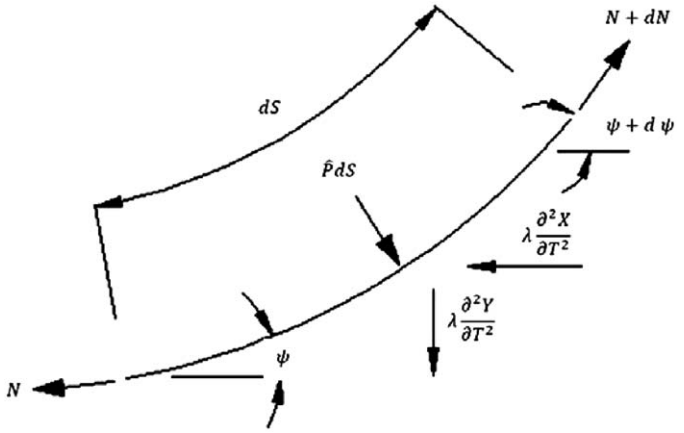

Fig. 2. Kinetic equilibrium diagram for a differential element of the membrane.

is B, the fluid pressure is $\hat{P}$, the pressure head is H_f, the density of the fluid is ρ, the mass per unit length of the tube is λ and the in-plain tension is $N(S,T)$.

For the range $0 \leq S \leq L$, geometrical relationships are

$$\frac{\partial X}{\partial S} = \cos(\psi), \quad \frac{\partial Y}{\partial S} = \sin(\psi). \tag{1a, b}$$

Consider the free body diagram shown in Fig. 2. Using d'Alembert's principle, the mass of the body and its acceleration can be regarded as a force in the opposite direction of the acceleration (Bedford and Fowler, 1999). Dynamic equilibrium of forces in the tangential and normal directions yields

$$\lambda\frac{\partial^2 X}{\partial T^2}\cos(\psi) + \lambda\frac{\partial^2 Y}{\partial T^2}\sin(\psi) = \frac{\partial N}{\partial S}, \tag{2a}$$

$$\lambda\frac{\partial^2 Y}{\partial T^2}\cos(\psi) - \lambda\frac{\partial^2 X}{\partial T^2}\sin(\psi) = N\frac{\partial \psi}{\partial S} - \hat{P}. \tag{2b}$$

The coordinates are written in the form

$$X(S,T) = X_e(S) + V_t(S,T)\cos\psi_s - V_n(S,T)\sin\psi_s, \tag{3}$$

$$Y(S,T) = Y_e(S) + V_t(S,T)\sin\psi_s + V_n(S,T)\cos\psi_s, \tag{4}$$

where V_t^d, V_n^d and ψ_s are tangential displacement, normal displacement and tangential angle of the membrane with the horizontal direction in the equilibrium configuration. Substituting Eqs. (3) and (4) in Eqs. (2a) and (2b), leads to

$$\lambda\frac{\partial^2 V_t}{\partial T^2}\cos(\psi-\psi_s) + \lambda\frac{\partial^2 V_n}{\partial T^2}\sin(\psi-\psi_s) = \frac{\partial N}{\partial S}, \tag{5}$$

$$\lambda\frac{\partial^2 V_n}{\partial T^2}\cos(\psi-\psi_s) - \lambda\frac{\partial^2 V_t}{\partial T^2}\sin(\psi-\psi_s) = N\frac{\partial\psi}{\partial S} - \hat{P}. \tag{6}$$

Assuming the displacements from the equilibrium configuration to be sufficiently small, $\cos(\psi-\psi_s) = 1$ and $\sin(\psi-\psi_s) = (\psi-\psi_s)$, Eqs. (5) and (6) can be rewritten as

$$\lambda\frac{\partial^2 V_t}{\partial T^2} + \lambda\frac{\partial^2 V_n}{\partial T^2}(\psi-\psi_s) = \frac{\partial N}{\partial S}, \tag{7}$$

$$\lambda\frac{\partial^2 V_n}{\partial T^2} - \lambda\frac{\partial^2 V_t}{\partial T^2}(\psi-\psi_s) = N\frac{\partial\psi}{\partial S} - \hat{P}. \tag{8}$$

If V_n, V_t and $(\psi-\psi_s)$ are of order ε (with $\varepsilon \ll 1$), then the terms $\partial^2 V_t/\partial T^2(\psi-\psi_s)$ and $\partial^2 V_n/\partial T^2(\psi-\psi_s)$ are of order ε^2, and we can neglect these terms in Eqs. (7) and (8). The resultant equations are

$$\lambda\frac{\partial^2 V_t}{\partial T^2} = \frac{\partial N}{\partial S}, \quad \lambda\frac{\partial^2 V_n}{\partial T^2} = N\frac{\partial\psi}{\partial S} - \hat{P}. \tag{9,10}$$

The variations of the fluid pressure can be divided into two parts, one contains a time-dependent part P_d and the other one contains the static value $P_s = \rho g(H_f + Y)$. To simplify these equations, the following nondimensional quantities are defined:

$$\begin{aligned} &x = \frac{Y}{B}, \quad y = \frac{Y}{B}, \quad v_t^d = \frac{V_t}{B}, \quad v_n^d = \frac{V_n}{B}, \quad s = \frac{S}{B}, \quad l = \frac{L}{B}, \\ &n = \frac{N}{\rho g B^2}, \quad \hat{P} = \frac{\hat{P}}{\rho g B}, \quad t = T\sqrt{\frac{g}{B}}, \quad h_f = \frac{H_f}{B}, \quad \omega = \Omega\sqrt{\frac{B}{g}}, \quad \eta = \frac{\lambda}{\rho B} \end{aligned} \tag{11}$$

where Ω is a vibration frequency. Based on Eqs. (1), (9) and (10), the static and dynamic behaviors of the membrane can be obtained.

3. Static analysis

Considering the time-independent terms in Eqs. (2a) and (2b) and neglecting the membrane weight with respect to the fluid weight, the following nondimensional governing equations for the static analysis can be obtained:

$$\frac{dx_e}{ds} - \cos(\psi_s) = 0, \quad \frac{dy_e}{ds} - \sin(\psi_s) = 0, \tag{12,13}$$

$$\frac{dn}{ds} = 0, \quad n\frac{d\psi_s}{ds} - (h_f + y_e) = 0, \tag{14,15}$$

where x_e and y_e are the coordinates of the membrane in equilibrium position. ψ_s is the tangential angle of the membrane with the horizontal direction in the equilibrium configuration. For determining the equilibrium shape of the fluid–membrane system, the system of differential Eqs. (12)–(15) must be solved. Eq. (14) shows that the tension in the membrane is independent of the arc length. In view of this, using Eqs. (12)–(15) and the boundary conditions at $s = 0$

$$x_e(s=0) = 0, \quad y_e(s=0) = 0, \quad \psi_s(s=0) = -\psi_w, \tag{16}$$

the following relations can be derived (Ghavanloo and Daneshmand, 2009):

$$y_e(\psi_s) = -h_f + \sqrt{h_f^2 + 2n_0(\cos(\psi_w) - \cos(\psi_s))}, \tag{17}$$

$$x_e(\psi_s) = \left(n_0 \int_{-\psi_w}^{\psi_s} \frac{\cos(\beta)}{\sqrt{h_f^2 + 2n_0(\cos(\psi_w) - \cos(\beta))}} d\beta \right), \tag{18}$$

where n_0 is the nondimensional tension. These equations define the equilibrium shape of the fluid-filled membrane as a function of two unknown parameters n_0 and ψ_w. Assuming the symmetric shape of the membrane and noting that

$$x_e(\psi_s = \psi_w) = 1, \quad s(\psi_s = \psi_w) = l, \tag{19}$$

the two unknown parameters can be evaluated as

$$n_0 \int_{-\psi_w}^{\psi_w} \frac{\cos(\beta)}{\sqrt{h_f^2 + 2n_0(\cos(\psi_w) - \cos(\beta))}} d\beta = 1, \tag{20}$$

$$n_0 \int_{-\psi_w}^{\psi_w} \frac{1}{\sqrt{h_f^2 + 2n_0(\cos(\psi_w) - \cos(\beta))}} d\beta = l. \tag{21}$$

It should be noted that Eqs. (18), (20) and (21) contain elliptic integrals. Therefore, to obtain the equilibrium shape of the fluid-filled membrane, these equations must be solved numerically.

Typical equilibrium shapes of the membrane are shown in Figs. 3 and 4. In Fig. 3, the nondimensional pressure head (h_f) is fixed at 1.0 and the cross-sections of the membrane are shown for four nondimensional membrane length $l = 1.05$, 1.15, 1.25 and 1.35. In Fig. 4, l is fixed at 1.25 and $h_f = 1$, 1.5, and 2.0. In Fig. 4, it can be seen that the equilibrium shape of the membrane for different values of the pressure head is coincident. Inextensibility of the membrane is responsible for this important result. The angle at the right support (ψ_w), increases as l increases (Fig. 3). This behavior is illustrated in Fig. 5, where h_f is fixed. The nondimensional tension n_0 is also plotted in this figure. The tension initially decreases as the membrane length increases, but then slowly increases. This fact can be described by the following statements. The weight of the fluid is carried by the vertical component of the membrane tension at the supports, $2n_0 \sin \psi_w$. For the membrane length $l \approx 1$, the tangential angle of the bottom membrane is small and the membrane tension should be large enough to be able to carry the fluid weight. For larger membrane lengths, $l > 1$, the tangential angle of the bottom membrane increases and so the membrane tension can decrease in magnitude.

It should be noted that, if the length of the bottom membrane is specified, the angle at the right support is constant for all values of the pressure head h_f. In this case, the nondimensional tension in the membrane is plotted for different

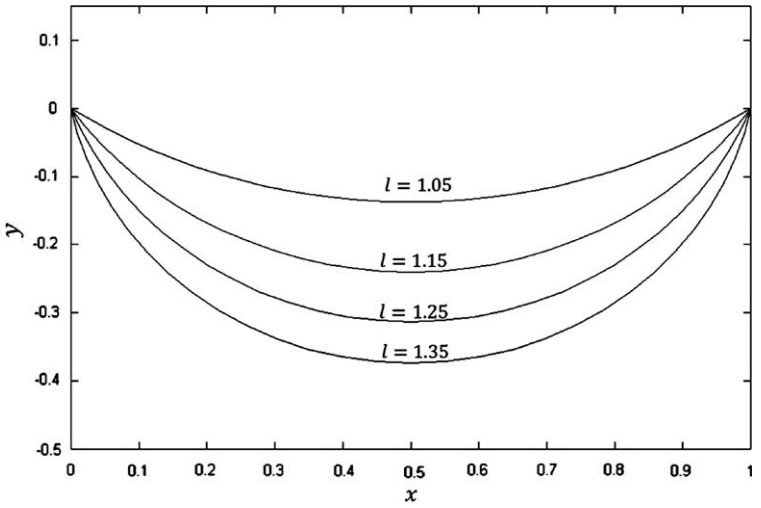

Fig. 3. Equilibrium shapes of the membrane for $h_f = 1$ and $l = 1.05$, 1.15, 1.25 and 1.35.

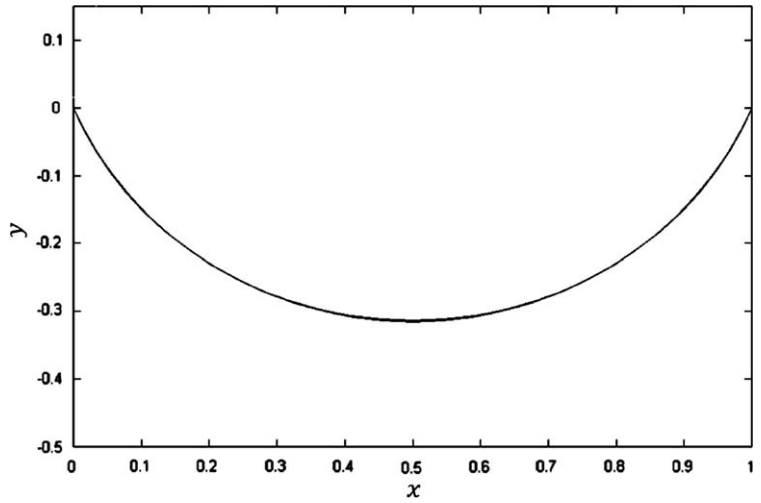

Fig. 4. Equilibrium shapes of the membrane for $l = 1.25$ and $h_f = 1$, 1.5 and 2.

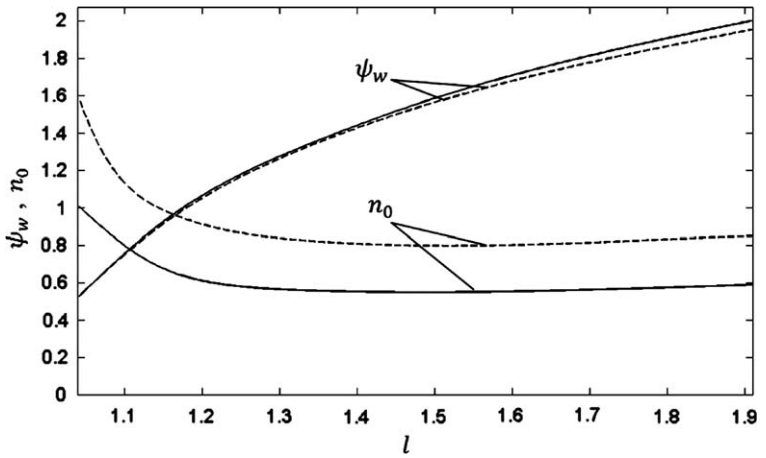

Fig. 5. Variation of the base angle and the nondimensional tension with the nondimensional membrane length:——, $h_f = 1$;– – –, $h_f = 1.5$.

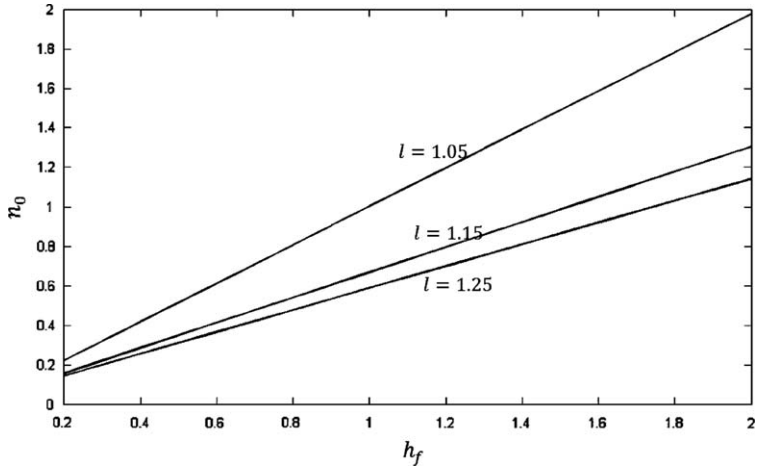

Fig. 6. Variation of the nondimensional tension with the nondimensional pressure head and the nondimensional membrane length.

pressure heads (Fig. 6). It can be seen that the tension in the membrane is varied linearly with respect to the fluid pressure head. In fact by writing the force balance in the vertical direction, we can derive the relation $n_0=[\int_0^1 y_e dx_e+h_f]/2\sin\psi_w$ between h_f and n_0. Using this relation and the results shown in Fig. 4, the variation of the membrane tension with h_f as given in Fig. 6 is satisfactory.

4. Dynamic analysis

4.1. Solid domain

In order to analyze the vibrations of the membrane about its equilibrium configuration, the equations of motion in the tangential and normal directions can be written in nondimensional form as

$$\eta\frac{\partial^2 v_t^d}{\partial t^2}=\frac{\partial(n_d+n_0)}{\partial s}=\frac{\partial n_d}{\partial s}, \tag{22a}$$

$$\eta\frac{\partial^2 v_n^d}{\partial t^2}=(n_d+n_0)\frac{\partial\psi}{\partial s}-\hat{p}=(n_d+n_0)\frac{\partial\psi}{\partial s}-(p_s+p_d), \tag{22b}$$

where v_t^d, v_n^d and n_d are tangential displacement, normal displacement and additional tension in the membrane, respectively. To eliminate n_d, one can solve Eq. (22b) for n_d, differentiate the result with respect to s, substitute it into Eq. (22a), and multiply by $(\partial\psi/\partial s)^2$.The resultant equation is

$$\eta\frac{\partial^3 v_n^d}{\partial t^2\partial s}\frac{\partial\psi}{\partial s}=\eta\frac{\partial^2 v_t^d}{\partial t^2}\left(\frac{\partial\psi}{\partial s}\right)^2+\eta\frac{\partial^2 v_n^d}{\partial t^2}\frac{\partial^2\psi}{\partial s^2}+(p_s+p_d)\frac{\partial^2\psi}{\partial s^2}-\frac{\partial(p_s+p_d)}{\partial s}\frac{\partial\psi}{\partial s}. \tag{23}$$

It is convenient to define the quantities

$$\mathfrak{A}=\frac{\partial\psi_s}{\partial s},\quad \mathfrak{B}=\frac{\partial^2\psi_s}{\partial s^2},\quad \mathfrak{C}=\frac{\partial^3\psi_s}{\partial s^3},\quad \mathfrak{D}=\frac{\partial^4\psi_s}{\partial s^4}. \tag{24}$$

To simplify Eq. (23), we need to use two parameters: dynamic curvature and tangential strain. The dynamic curvature can be written in the form

$$\frac{\partial\psi}{\partial s}=\mathfrak{A}+\frac{\frac{\partial^2 v_n^d}{\partial s^2}+\mathfrak{A}^2 v_n^d+\mathfrak{B}v_t^d}{1+\frac{\partial v_t^d}{\partial s}-\mathfrak{A}v_n^d}. \tag{25}$$

A derivation of this relation is presented in Appendix A. The tangential strain (ε_ψ) can be written in the form (Kelkar and Sewell, 1987)

$$\varepsilon_\psi=\frac{\left(\frac{\partial v_t^d}{\partial\psi}-v_n^d\right)}{R}, \tag{26}$$

where R is the radius of curvature. Due to the assumption of inextensibility, the tangential strain is zero. Using this fact and linearizing Eq. (25), one obtains the relation

$$v_n^d=\mathfrak{A}^{-1}\frac{\partial v_t^d}{\partial s}. \tag{27}$$

Eqs. (25) and (27) are now substituted in Eq. (23). In addition, from Eqs. (15) and (24) it follows that

$$p_s=\mathfrak{A}n_0,\quad \frac{\partial p_s}{\partial s}=\mathfrak{B}n_0. \tag{28}$$

The equation of motion can be derived by using the above relations, neglecting the higher order terms and linearizing, yielding

$$\frac{\eta}{n_0}\left(\mathfrak{A}^2\frac{\partial^2 v_t^d}{\partial t^2}+2\mathfrak{A}^{-1}\mathfrak{B}\frac{\partial^3 v_t^d}{\partial t^2\partial s}-\frac{\partial^4 v_t^d}{\partial t^2\partial s^2}\right)+\frac{\partial^4 v_t^d}{\partial s^4}+a_1\frac{\partial^3 v_t^d}{\partial s^3}+a_2\frac{\partial^2 v_t^d}{\partial s^2}+a_3\frac{\partial v_t^d}{\partial s}+a_4 v_t^d=\frac{1}{n_0}\left(\mathfrak{A}\frac{\partial p_d}{\partial s}-\mathfrak{B}p_d\right), \tag{29}$$

where

$$a_1 = -4\mathfrak{A}^{-1}\mathfrak{B}, \quad a_2 = 8\mathfrak{A}^{-2}\mathfrak{B}^2 + \mathfrak{A}^2 - 3\mathfrak{C}\mathfrak{A}^{-1},$$
$$a_3 = 7\mathfrak{B}\mathfrak{C}\mathfrak{A}^{-2} - 8\mathfrak{A}^{-3}\mathfrak{B}^3 + \mathfrak{A}\mathfrak{B} - \mathfrak{D}\mathfrak{A}^{-1}, \quad a_4 = \mathfrak{A}\mathfrak{C} - \mathfrak{B}^2. \tag{30}$$

The boundary conditions of the membrane are given by

$$v_t^d = 0 \quad at\ s = 0, l, \tag{31a}$$
$$v_n^d = \mathfrak{A}^{-1}\frac{\partial v_t^d}{\partial s} = \frac{\partial v_t^d}{\partial s} = 0 \quad at\ s = 0, l. \tag{31b}$$

4.2. Fluid domain

The liquid in this system is assumed to be incompressible, inviscid and irrotational. In the absence of external forces, the governing differential equation for free small amplitude motion of the liquid in terms of the nondimensional pressure variable is

$$\nabla^2(p_d + p_s) = \nabla^2 p_d = 0, \tag{32}$$

in which ∇^2 is the Laplace operator. Eq. (32) is solved using the finite element technique, with the appropriate time-dependent boundary conditions as specified below.

(a) *On the fluid–structure interface:*

$$\frac{\partial p_d}{\partial n} = \frac{\partial^2 v_n^d}{\partial t^2} = \mathfrak{A}^{-1}\frac{\partial^3 v_t^d}{\partial t^2 \partial s} \quad \text{on} \quad \boldsymbol{\Gamma}_s, \tag{33}$$

where n is the direction cosine vector for an outward pointing normal to the fluid region.

(b) *On the liquid free surface:*

Neglecting the free-surface wave, the free surface condition can be written as

$$p_d = 0 \quad \text{at} \quad \boldsymbol{\Gamma}_0. \tag{34}$$

(c) *On the rigid walls:*

$$\frac{\partial p_d}{\partial n} = 0 \quad \text{at} \quad x = 0, 1. \tag{35}$$

5. Finite element procedure

5.1. Weak formulation

For developing the weak form of Eqs. (29) and (32), we multiply the equations (29) and (32) by the test functions ξ and ζ such that $\xi = 0$ and $\partial\xi/\partial s = 0$ at $s = 0,l$, $\zeta = 0$ on Γ_0 and integrate over the element domains. Using integration by parts on some of the terms and the boundary conditions we obtain

$$\int_{s_1^e}^{s_2^e}\left(\frac{\eta}{n_0}\left((\mathfrak{A}^e)^2\xi\frac{\partial^2 v_t^d}{\partial t^2} - 2(\mathfrak{A}^e)^{-1}(\mathfrak{B}^e)\frac{\partial\xi}{\partial s}\frac{\partial^2 v_t^d}{\partial t^2} + \frac{\partial\xi}{\partial s}\frac{\partial^3 v_t^d}{\partial t^2\partial s}\right) + \frac{\partial^2\xi}{\partial s^2}\frac{\partial^2 v_t^d}{\partial s^2} - a_1^e\frac{\partial\xi}{\partial s}\frac{\partial^2 v_t^d}{\partial s^2}\right.$$
$$\left. - a_2^e\frac{\partial\xi}{\partial s}\frac{\partial v_t^d}{\partial s} + a_3^e\xi\frac{\partial v_t^d}{\partial s} + a_4^e\xi v_t^d\right)ds + \xi\left(\frac{\eta}{n_0}\left(2(\mathfrak{A}^e)^{-1}(\mathfrak{B}^e)\frac{\partial^2 v_t^d}{\partial t^2} - \frac{\partial^3 v_t^d}{\partial t^2\partial s}\right) + \frac{\partial^3 v_t^d}{\partial s^3} + a_1^e\frac{\partial^2 v_t^d}{\partial s^2} + a_2^e\frac{\partial^2 v_t^d}{\partial s}\right)$$
$$\left. - \mathfrak{A}^e p_d\right)\right|_{s_1^e}^{s_2^e} - \left(\frac{\partial\xi}{\partial s}\frac{\partial^2 v_t^d}{\partial s^2}\right)\Bigg|_{s_1^e}^{s_2^e} = -\frac{1}{n_0}\int_{s_1^e}^{s_2^e}\left[(\mathfrak{A}^e)\frac{\partial\xi}{\partial s} + (\mathfrak{B}^e)\xi\right]p_d ds, \tag{36}$$

$$\int_{\Omega_f^e}(\nabla\zeta)(\nabla p_d)d\Omega = \oint_{\boldsymbol{\Gamma}_f^e}\zeta\frac{\partial p_d}{\partial n}d\boldsymbol{\Gamma}_f = \oint_{\boldsymbol{\Gamma}_s^e}\zeta(\mathfrak{A}^e)^{-1}\frac{\partial^3 v_t^d}{\partial t^2\partial s}d\boldsymbol{\Gamma}_s + \oint_{\boldsymbol{\Gamma}_f^e/\boldsymbol{\Gamma}_s^e}\zeta\frac{\partial p_d}{\partial n}d\boldsymbol{\Gamma}_f. \tag{37}$$

The variational formulation of the fluid–structure interaction problem is to find v_t^d and p_d such that Eqs. (36) and (37) are satisfied for all ξ and ζ including appropriate boundary conditions.

5.2. Finite element discretization

Using the finite element discretization procedure (Bathe, 1995), one can express the displacement v_t^d and the dynamic pressure p_d, in terms of the standard isoparametric interpolation functions as

$$(v_t^d)^e = \mathbf{\Phi^e U^e}, \tag{38}$$

$$(p_d)^e = \mathbf{\Psi^e p^e}, \tag{39}$$

where $\mathbf{\Phi^e}$ and $\mathbf{\Psi^e}$ are shape functions for the membrane and the fluid domain, respectively. These functions relate the displacement $(v_t^d)^e$ and $(p_d)^e$ to the nodal displacements $\mathbf{U^e}$ and nodal dynamic pressure $\mathbf{p^e}$ and are defined as

$$\mathbf{\Phi^e} = \left[\phi_1^e \phi_2^e \boldsymbol{\phi}_3^e \phi_4^e\right], \quad \mathbf{U^e} = \left[u_1^e u_2^e u_3^e u_4^e\right]^{\mathrm{T}}, \tag{40}$$

$$\mathbf{\Psi^e} = \left[\psi_1^e \psi_2^e \ldots \psi_{N_f}^e\right], \mathbf{p^e} = \left[p_1^e p_2^e \ldots p_{N_f}^e\right]^{\mathrm{T}}, \tag{41}$$

where N_f is number of nodes for the fluid elements. Also, ϕ_i^e are Hermite cubic interpolation (or cubic spline) functions. These interpolation functions can be expressed in terms of the local coordinate s (with $s_2^e = s_1^e + h^e$):

$$\begin{aligned} &\phi_1^e = 1-3\left(\frac{s}{h^e}\right)^2 + 2\left(\frac{s}{h^e}\right)^3, \quad \phi_2^e = -s\left(1-\frac{s}{h^e}\right)^2, \\ &\phi_3^e = 3\left(\frac{s}{h^e}\right)^2 - 2\left(\frac{s}{h^e}\right)^3, \quad \phi_4^e = -s\left(\left(\frac{s}{h^e}\right)^2 - \frac{s}{h^e}\right). \end{aligned} \tag{42}$$

Choosing ξ according to the Galerkin method, the discretized forms of different terms in Eq. (36) become

$$\begin{aligned} &\int_{s_1^e}^{s_2^e} \frac{\eta}{n_0}\left((\mathfrak{A}^e)^2 \xi \frac{\partial^2 v_t^d}{\partial t^2} - 2(\mathfrak{A}^e)^{-1}(\mathfrak{B}^e)\frac{\partial \xi}{\partial s}\frac{\partial^2 v_t^d}{\partial t^2} + \frac{\partial \xi}{\partial s}\frac{\partial^3 v_t^d}{\partial t^2 \partial s}\right) ds + \xi \frac{\eta}{n_0}\left(2(\mathfrak{A}^e)^{-1}(\mathfrak{B}^e)\frac{\partial^2 v_t^d}{\partial t^2} - \frac{\partial^3 v_t^d}{\partial t^2 \partial s}\right)\Big|_{s_1^e}^{s_2^e} \\ &= \left(\int_{s_1^e}^{s_2^e} \frac{\eta}{n_0}\left((\mathfrak{A}^e)^2 (\mathbf{\Phi^e})^{\mathrm{T}}\mathbf{\Phi^e} - 2(\mathfrak{A}^e)^{-1}(\mathfrak{B}^e)\left(\frac{\partial \mathbf{\Phi^e}}{\partial s}\right)^{\mathrm{T}}\mathbf{\Phi^e} + \left(\frac{\partial \mathbf{\Phi^e}}{\partial s}\right)^{\mathrm{T}}\frac{\partial \mathbf{\Phi^e}}{\partial s}\right) ds \right. \\ &\quad \left. + \frac{\eta}{n_0}\left(2(\mathfrak{A}^e)^{-1}(\mathfrak{B}^e)(\mathbf{\Phi^e})^{\mathrm{T}}\mathbf{\Phi^e} - (\mathbf{\Phi^e})^{\mathrm{T}}\frac{\partial \mathbf{\Phi^e}}{\partial s}\right)\Big|_{s_1^e}^{s_2^e}\right)\ddot{\mathbf{U}}^{\mathbf{e}}, \end{aligned} \tag{43}$$

$$\begin{aligned} &\int_{s_1^e}^{s_2^e}\left(\frac{\partial^2 \xi}{\partial s^2}\frac{\partial^2 v_t^d}{\partial s^2} - a_1^e \frac{\partial \xi}{\partial s}\frac{\partial^2 v_t^d}{\partial s^2} - a_2^e \frac{\partial \xi}{\partial s}\frac{\partial v_t^d}{\partial s} + a_3^e \xi \frac{\partial v_t^d}{\partial s} + a_4^e \xi v_t^d\right) ds \\ &\quad + \xi\left(\frac{\partial^3 v_t^d}{\partial s^3} + a_1^e \frac{\partial^2 v_t^d}{\partial s^2} + a_2^e \frac{\partial v_t^d}{\partial s} - \mathfrak{A}^e p_d\right)\Big|_{s_1^e}^{s_2^e} - \left(\frac{\partial \xi}{\partial s}\frac{\partial^2 v_t^d}{\partial s^2}\right)\Big|_{s_1^e}^{s_2^e} \\ &= \left(\int_{s_1^e}^{s_2^e}\left(\left(\frac{\partial^2 \mathbf{\Phi^e}}{\partial s^2}\right)^{\mathrm{T}}\frac{\partial^2 \mathbf{\Phi^e}}{\partial s^2} - a_1^e\left(\frac{\partial \mathbf{\Phi^e}}{\partial s}\right)^{\mathrm{T}}\frac{\partial^2 \mathbf{\Phi^e}}{\partial s^2} - a_2^e\left(\frac{\partial \mathbf{\Phi^e}}{\partial s}\right)^{\mathrm{T}}\frac{\partial \mathbf{\Phi^e}}{\partial s} + a_3^e(\mathbf{\Phi^e})^{\mathrm{T}}\frac{\partial \mathbf{\Phi^e}}{\partial s}\right.\right. \\ &\quad \left.\left. + a_4^e(\mathbf{\Phi^e})^{\mathrm{T}}\mathbf{\Phi^e}\right) ds + (\mathbf{\Phi^e})^{\mathrm{T}}\left(\frac{\partial^3 \mathbf{\Phi^e}}{\partial s^3} + a_1^e\frac{\partial^2 \mathbf{\Phi^e}}{\partial s^2} + a_2^e\frac{\partial \mathbf{\Phi^e}}{\partial s}\right)\Big|_{s_1^e}^{s_2^e} - \left(\frac{\partial (\mathbf{\Phi^e})^{\mathrm{T}}}{\partial s}\frac{\partial^2 \mathbf{\Phi^e}}{\partial s^2}\right)\Big|_{s_1^e}^{s_2^e}\right)\mathbf{U^e} - \left((\mathbf{\Phi^e})^{\mathrm{T}}(\mathfrak{A}^e\mathbf{\Psi^e})\Big|_{s_1^e}^{s_2^e}\right)\mathbf{p^e}, \end{aligned} \tag{44}$$

$$\frac{1}{n_0}\int_{s_1^e}^{s_2^e}\left[(\mathfrak{A}^e)\frac{\partial \xi}{\partial s} + (\mathfrak{B}^e)\xi\right] p_d ds = \left(\frac{1}{n_0}\int_{s_1^e}^{s_2^e}\left[(\mathfrak{A}^e)\left(\frac{\partial \mathbf{\Phi^e}}{\partial s}\right)^{\mathrm{T}} + (\mathfrak{B}^e)(\mathbf{\Phi^e})^{\mathrm{T}}\right]\mathbf{\Psi^e} ds\right)\mathbf{p^e}. \tag{45}$$

Substituting these relations into Eq. (36), the following equation for the membrane domain is obtained

$$\left(\mathbf{M_s^e} + \mathbf{m_b^e}\right)\ddot{\mathbf{U}}^{\mathbf{e}} + (\mathbf{K_s^e} + \mathbf{F^e})\mathbf{U^e} = (-\mathbf{T^e} + \mathbf{S^e})\mathbf{p^e}, \tag{46}$$

in which $\mathbf{U^e}$ is the matrix including the unknown nodal values of the membrane tangential displacement in the element and

$$\mathbf{M_s^e} = \int_{s_1^e}^{s_2^e}\frac{\eta}{n_0}\left((\mathfrak{A}^e)^2(\mathbf{\Phi^e})^{\mathrm{T}}\mathbf{\Phi^e} - 2(\mathfrak{A}^e)^{-1}(\mathfrak{B}^e)\left(\frac{\partial \mathbf{\Phi^e}}{\partial s}\right)^{\mathrm{T}}\mathbf{\Phi^e} + \left(\frac{\partial \mathbf{\Phi^e}}{\partial s}\right)^{\mathrm{T}}\frac{\partial \mathbf{\Phi^e}}{\partial s}\right) ds, \tag{47}$$

$$\mathbf{m_b^e} = \frac{\eta}{n_0}\left(2(\mathfrak{A}^e)^{-1}(\mathfrak{B}^e)(\mathbf{\Phi^e})^{\mathrm{T}}\mathbf{\Phi^e} - (\mathbf{\Phi^e})^{\mathrm{T}}\frac{\partial \mathbf{\Phi^e}}{\partial s}\right)\Big|_{s_1^e}^{s_2^e}, \tag{48}$$

$$\mathbf{K_s^e} = \int_{s_1^e}^{s_2^e}\left(\left(\frac{\partial^2 \mathbf{\Phi^e}}{\partial s^2}\right)^{\mathrm{T}}\frac{\partial^2 \mathbf{\Phi^e}}{\partial s^2} - a_1^e\left(\frac{\partial \mathbf{\Phi^e}}{\partial s}\right)^{\mathrm{T}}\frac{\partial^2 \mathbf{\Phi^e}}{\partial s^2} - a_2^e\left(\frac{\partial \mathbf{\Phi^e}}{\partial s}\right)^{\mathrm{T}}\frac{\partial \mathbf{\Phi^e}}{\partial s} + a_3^e(\mathbf{\Phi^e})^{\mathrm{T}}\frac{\partial \mathbf{\Phi^e}}{\partial s} + a_4^e(\mathbf{\Phi^e})^{\mathrm{T}}\mathbf{\Phi^e}\right) ds, \tag{49}$$

$$\mathbf{T^e} = \frac{1}{n_0}\int_{s_1^e}^{s_2^e}\left[(\mathfrak{A}^e)\left(\frac{\partial \mathbf{\Phi^e}}{\partial s}\right)^{\mathrm{T}} + (\mathfrak{B}^e)(\mathbf{\Phi^e})^T\right]\mathbf{\Psi^e}\, ds, \tag{50}$$

$$\mathbf{F^e} = (\mathbf{\Phi^e})^T\left(\frac{\partial^3 \mathbf{\Phi^e}}{\partial s^3} + a_1^e\frac{\partial^2 \mathbf{\Phi^e}}{\partial s^2} + a_2^e\frac{\partial \mathbf{\Phi^e}}{\partial s}\right)\Big|_{s_1^e}^{s_2^e} - \left(\frac{\partial(\mathbf{\Phi^e})^T}{\partial s}\frac{\partial^2 \mathbf{\Phi^e}}{\partial s^2}\right)\Big|_{s_1^e}^{s_2^e}, \tag{51}$$

$$\mathbf{S^e} = \left((\mathbf{\Phi^e})^T(\mathfrak{A}^e\mathbf{\Psi^e})\Big|_{s_1^e}^{s_2^e}\right). \tag{52}$$

The related equation for the fluid domain can also be written as

$$(\mathbf{K_f^e} + \mathbf{Q^e})\mathbf{p^e} = \mathbf{Q_{mf}^e}\ddot{\mathbf{U}}^{\mathbf{e}}, \tag{53}$$

where $\mathbf{K_f^e}$ is fluid element system matrix and $\mathbf{Q_{mf}^e}$ is the load due to the fluid–solid interaction defined as

$$\mathbf{K_f^e} = \left(\int_{\Omega_f^e}(\nabla\mathbf{\Psi^e})^T(\nabla\mathbf{\Psi^e})\, d\Omega\right), \tag{54}$$

$$\mathbf{Q_{mf}^e} = \oint_{S_m}(\mathfrak{A}^e)^{-1}(\mathbf{\Psi^e})^T\frac{\partial \mathbf{\Phi^e}}{\partial s}\, ds, \tag{55}$$

$$\mathbf{Q^e} = \oint_{\Gamma_f^e/\Gamma_s^e}(\mathbf{\Psi^e})^T\frac{\partial \mathbf{\Psi^e}}{\partial n}\, d\boldsymbol{\Gamma}_f. \tag{56}$$

It should be noted that two types of elements are used in the discretization of the fluid region: (*i*) linear triangular elements and (*ii*) linear rectangular elements. Combining Eqs. (46) and (52), for the fluid and the membrane elements and using the assembling procedure, the following system of equations can be obtained:

$$\begin{bmatrix}\mathbf{M_s} & \mathbf{0}\\ -\mathbf{Q_{mf}} & \mathbf{0}\end{bmatrix}\begin{Bmatrix}\ddot{\mathbf{U}}\\ \ddot{\mathbf{p}}\end{Bmatrix} + \begin{bmatrix}\mathbf{K_s} & \mathbf{T}\\ \mathbf{0} & \mathbf{K_f}\end{bmatrix}\begin{Bmatrix}\mathbf{U}\\ \mathbf{p}\end{Bmatrix} = \begin{Bmatrix}\mathbf{0}\\ \mathbf{0}\end{Bmatrix}. \tag{57}$$

It should be noted that the matrices $\mathbf{m_b^e}$, $\mathbf{F^e}$, $\mathbf{S^e}$ and $\mathbf{Q^e}$ are dropped in the assemblage process, because the elements of these matrices in adjacent elements have approximately the same value, with negative sign. We can eliminate the pressure $\mathbf{p}$ to yield

$$(\mathbf{M_s} + \mathbf{M_a})\ddot{\mathbf{U}} + \mathbf{K_s}\mathbf{U} = \mathbf{0}, \tag{58}$$

where

$$\mathbf{M_a} = \mathbf{T}(\mathbf{K_f})^{-1}\mathbf{Q_{mf}} \tag{59}$$

is referred to as the added mass matrix. $\mathbf{M_a}$ has dimension equal to the number of structural degrees of freedom in the entire model. It should be noted that the mass and stiffness matrices in Eq. (58) for free vibration of the fluid–membrane system is nonsymmetric. To obtain the free-vibrations problem, we make the standard substitution

$$\mathbf{U} = \mathbf{u}e^{i\omega t} \tag{60}$$

into the transient response equations where $i = \sqrt{-1}$ and ω is the circular frequency. Substituting Eq. (60) in Eq.(58), a linear eigenvalue problem for a real, non-symmetric matrix is obtained.

6. Numerical results and discussion

A computer program based on finite element method is written according to the mathematical description given in the previous sections. In this section, the first six natural frequencies and mode shapes of a fluid–membrane system are obtained. The effects of different parameters including the membrane weight, the membrane length and the fluid level are also studied.

6.1. Convergence study

The convergence of the proposed method is studied by considering the natural frequencies of coupled vibration of a fluid–membrane system with the following properties: the distance between two rigid walls, B, is 20 cm, the membrane length, L, is 25 cm. The membrane is made of a material with a thickness of 1.04 mm and a density of 0.673 g/cm^3 and filled with water by the pressure head, $H_f = 30$ cm. The nondimensional parameters l, h_f and η defined in equation (3) are 1.25, 1.5, and 3.5×10^{-3}, respectively.

Table 1 gives the natural frequencies for the system for different numbers of elements, N, in the membrane domain. Moreover, the number of the fluid elements is also shown in the parenthesis. From the frequencies presented in this table, it is observed that the natural frequencies for $N = 150$ can be taken as the converged results. It should be noted that the desired relative error in convergence study is 0.0012% for the first mode.

6.2. Vibration mode shapes

The first six mode shapes of the membrane for $\eta = 0.0035$, $h_f = 1$ and $l = 1.25$ are shown in Fig. 7, along with equilibrium shape. The corresponding frequencies are $\omega = 6.8443$, 13.1762, 22.0166, 30.9830, 41.9075 and 53.1559, respectively. The six mode shapes fall into two categories: symmetric and antisymmetric. Symmetric and antisymmetric refer to the dynamic shape of the membrane being symmetrical or nonsymmetrical about the centerline of the equilibrium configuration. It is shown that the first mode of the system is antisymmetric whereas the second mode is symmetric, and so on. According to some experience in vibration analysis of different problems with symmetric geometry such as tight and sag string, the presence of symmetric and antisymmetric modes was predictable.

6.3. Effect of the membrane weight

Fig. 8 illustrates the effect of the membrane weight on the fluid-coupled natural frequencies of the fluid-filled rectangular container with a sagged bottom membrane. For the nondimensional membrane weight η in the range

Table 1
Convergence study of the nondimensional natural frequencies, effect of the number of elements in the membrane domain (N).

Mode	N (number of fluid elements)					
	8 (752)	16 (904)	32 (1208)	64 (1816)	128 (3032)	150 (3450)
1	8.4684	8.3891	8.3691	8.3641	8.3629	8.3628
2	16.4269	16.0349	15.9382	15.9141	15.9081	15.9075
3	28.7583	27.1126	26.7248	26.6294	26.6056	26.6034
4	42.9971	38.6776	37.7125	37.4787	37.4207	37.4155
5	63.5244	53.3728	51.2556	50.7520	50.6277	50.6165
6	85.9685	69.1868	65.2749	64.3661	64.1431	64.1230

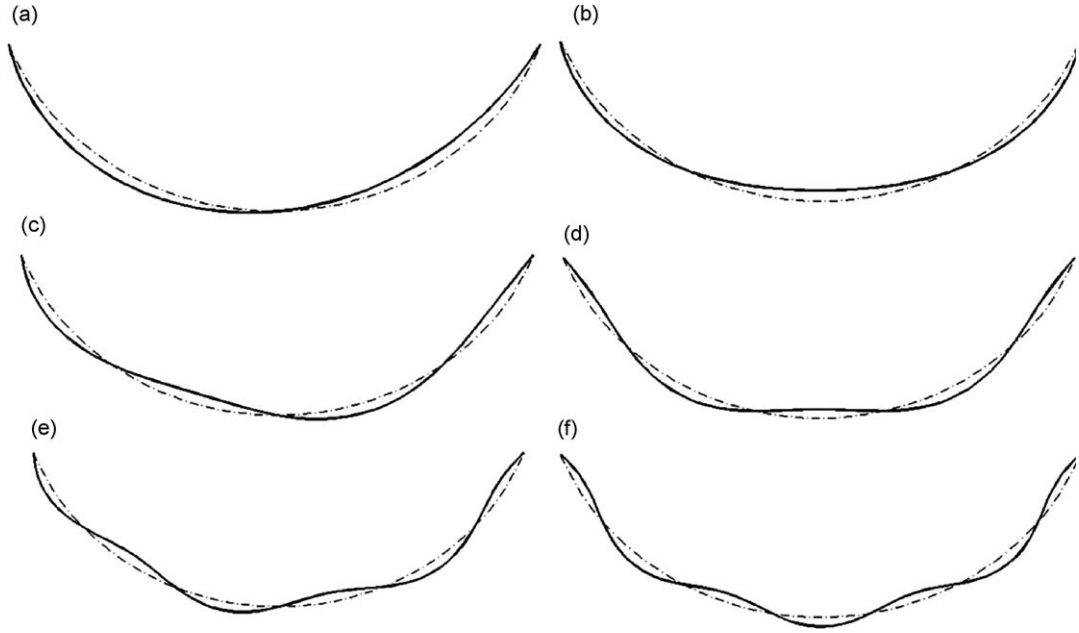

Fig. 7. The first six modes of the problem with $h_f = 1$, $l = 1.25$ and $\eta = 0.0035$: (a) first mode (antisymmetric); (b) second mode (symmetric mode); (c) third mode (antisymmetric); (d) forth mode (symmetric); (e) fifth mode (antisymmetric); (f) sixth mode (symmetric).

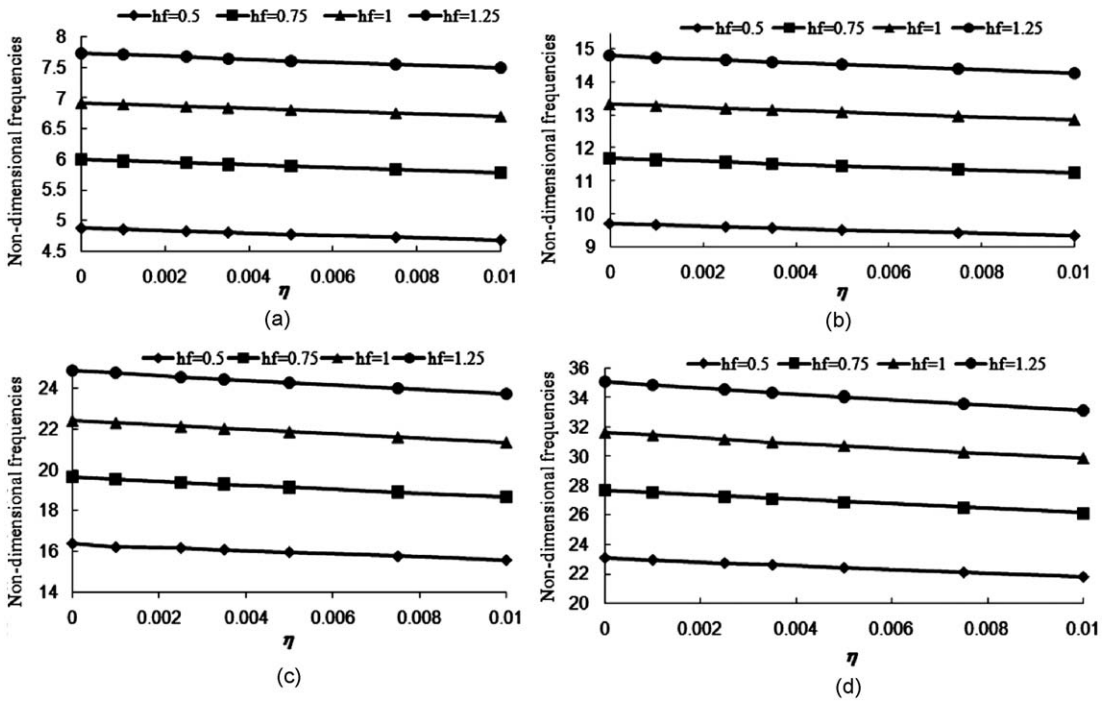

Fig. 8. Effect of membrane weight on natural frequencies of the fluid-filled rectangular container with a sagged bottom membrane for $l = 1.25$ and $h_f = 0.5$, 0.75, 1 and 1.25: (a) first natural frequency; (b) second natural frequency; (c) third natural frequency; (d) fourth natural frequency.

Table 2
Natural frequencies of the coupled system for two inertia ratios.

Membrane length	First mode		Second mode		Third mode		Fourth Mode	
	$\eta=0$	$\eta=0.01$	$\eta=0$	$\eta=0.01$	$\eta=0$	$\eta=0.01$	$\eta=0$	$\eta=0.01$
$l=1.05$	12.0934	11.8065	22.8617	22.0511	37.9898	36.1233	54.2066	50.8016
$l=1.15$	8.5626	8.3163	16.2134	15.6371	27.0619	25.7749	38.2735	36.0333
$l=1.25$	6.9258	6.7004	13.3481	12.8739	22.3966	21.3592	31.6322	29.8762
$l=1.35$	5.8385	5.6310	11.5302	11.1210	19.4216	18.5439	27.4539	25.9995

$0\leq\eta\leq0.01$, the variations of the first four nondimensional coupled frequencies for a specified membrane length $l=1.25$ and different nondimensional pressure head h_f are plotted in Fig. 8. It is clear that the natural frequencies of the fluid–membrane system gradually decrease as the nondimensional membrane weight increases. For a membrane weight η, the nondimensional natural frequencies decrease as the pressure head decreases. The differences among the results of the various modes of vibration are small, and it should be noted that the rate of decreasing the natural frequency increases as the number of modes increase.

To elucidate the small effect of the membrane weight on the natural frequencies, the numerical values of the frequencies for two extreme inertia ratios $\eta=0$, 0.01 ($0\leq\eta\leq0.01$) and pressure head = 1 are given in Table 2. It can be seen that the maximum decrease in frequencies occurs in the fourth mode for $l=1.05$ in which the frequency decreases about 6.28%. The same behavior can also be seen for other membrane lengths and pressure heads and therefore, the weight of the membrane does not have large affect on the natural frequencies. A change in the liquid density also has small effect on the natural frequencies. Moreover, it is obvious that the natural frequencies of the fluid–membrane system decrease as the membrane length increases.

It should be noted that if the above analysis is used for larger range of the membrane weights, the accuracy of the results may be decreased. This fact can be described by the following statements. The weight of the membrane is not included in obtaining the static equilibrium shape of the membrane. The static equilibrium shape of the bottom membrane has some effect on the dynamic analysis of the membrane. Therefore, if the inertia ratio increases, the assumption of neglected membrane weight is no longer valid and so the effect of the membrane weight must also be included in static and dynamic analysis.

6.4. *Effect of the membrane length*

The effect of the membrane length on the four lowest nondimensional natural frequencies for $\eta=0.0035$ and different pressure heads is shown in Fig. 9. It is well known that, generally, the natural frequencies of a system increase when its stiffness increases. In the present system, reduction of the membrane length is equivalent to increasing the in-plane tension and the stiffness of the system. Hence, as it can be seen from Fig. 9 and Table 2, the natural frequencies of the fluid–membrane system decrease when the length of the membrane increases. Moreover, with increasing the membrane length, the frequencies in higher mode numbers are much more decreased than those in lower mode numbers.

6.5. *Effect of the fluid level*

Fig. 9 shows the predicted natural frequencies of the fluid–membrane system as a function of the pressure head for various mode numbers. As can be observed from Fig. 9, the frequencies increase with increasing the pressure head. Consequently, the lowest wet frequencies occur when pressure head tends to zero. This conclusion can be reached by considering the inextensibility assumption for the membrane and the incompressibility assumption for the fluid. It should be noted that the equilibrium shape of the membrane does not change when the pressure head is changed (Fig. 4) and the relationship between the tension in the membrane and the pressure head is linear (Fig. 6). Also, it should be noted that the magnitude of the elements of the mass matrix ($\mathbf{M_s}$) and interaction matrix ($\mathbf{T}$) decrease with increasing pressure head, whereas the stiffness matrix of the membrane is fixed when the pressure head is changed (Eqs. (39)–(41)). Hence, the natural frequencies of fluid–membrane system increase as the pressure head increases.

At the end of this section, and regarding to the above discussion, an approximate relationship for calculating the natural frequency of the coupled system as a function of three unknown parameters can be proposed.

This relationship is

$$\omega = \overline{\omega}\sqrt{c_1 h_f + c_2}, \tag{61}$$

where $c_1 h_f + c_2$ is the slope-intercept form of n_0 shown in Fig. 6. This is called the slope-intercept form, because "c_1" is the slope and "c_2" gives the n_0-intercept. These constants can easily be found using Fig. 6. To evaluate $\overline{\omega}$, the following relation can be used:

$$\overline{\omega} = \frac{\omega_{\text{known}}}{\sqrt{c_1 (h_f)_{\text{known}} + c_2}}, \tag{62}$$

where ω_{known} is a known natural frequency of the coupled system for a specific pressure head $(h_f)_{\text{known}}$ (This frequency may be obtained by using any numerical method or even experiment.)

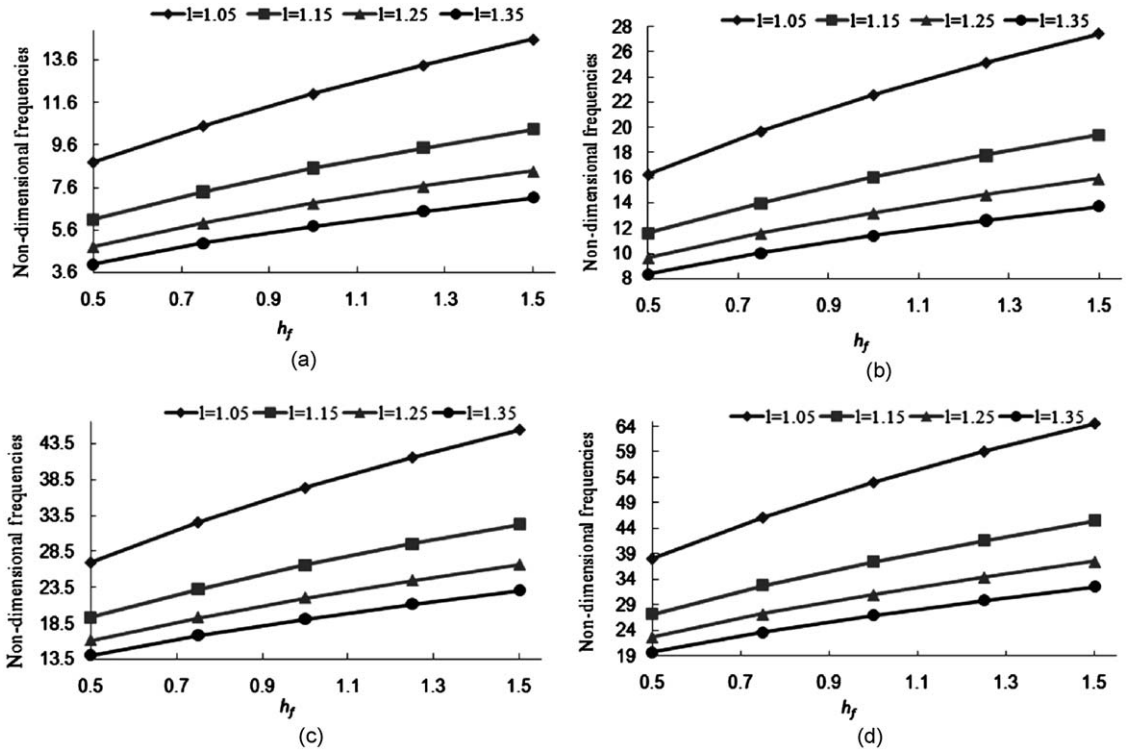

Fig. 9. Effect of the fluid level and the membrane length on natural frequencies of the fluid-filled rectangular container with a sagged bottom membrane for $\eta = 0.0035$ and $l = 1.05$, 1.15, 1.25 and 1.35: (a) first natural frequency; (b) second natural frequency; (c) third natural frequency; (d) fourth natural frequency.

Table (3a)
Comparison between the approximate formula and the finite element method (FEM) for $\eta = 0.0035$ and $l = 1.05$ ($c_1 = 0.983184$, $c_2 = 0.0229260$).

Pressure head	First mode		Second mode		Third mode		Fourth mode	
	$\omega_{\text{known}} = 8.7724$		$\omega_{\text{known}} = 19.6699$		$\omega_{\text{known}} = 37.3040$		$\omega_{\text{known}} = 58.9881$	
	Approximation	FEM	Approximation	FEM	Approximation	FEM	Approximation	FEM
$h_f = 0.50$	8.7724	8.7724	16.1809	16.2461	26.6765	26.9453	37.8159	38.0231
$h_f = 0.75$	10.6639	10.4863	19.6699	19.6699	32.4285	32.5289	45.9698	46.0947
$h_f = 1.00$	12.2671	11.9907	22.6271	22.5680	37.3040	37.3040	52.8811	52.9383
$h_f = 1.25$	13.6838	13.3328	25.2402	25.1275	41.6120	41.5388	58.9881	58.9881

Table (3b)
Comparison between the approximate formula and the finite element method (FEM) for $\eta = 0.0035$ and $l = 1.15$ ($c_1 = 0.639315$, $c_2 = 0.028021$).

Pressure head	First mode		Second mode		Third mode		Fourth mode	
	$\omega_{known} = 9.4377$		$\omega_{known} = 16.0045$		$\omega_{known} = 23.9945$		$\omega_{known} = 27.1508$	
	Approximation	FEM	Approximation	FEM	Approximation	FEM	Approximation	FEM
$hf = 0.50$	6.1187	6.0659	11.5552	11.6064	19.8601	19.3701	27.1508	27.1508
$hf = 0.75$	7.3925	7.3739	13.9570	13.9945	23.9945	23.9945	32.8028	32.7176
$hf = 1.00$	8.4770	8.4740	16.0045	16.0045	27.5144	26.5899	37.6150	37.4427
$hf = 1.25$	9.4377	9.4377	17.8182	17.7768	30.6326	29.5442	41.8778	41.6251

The results obtained by using this approximate formula are compared with those obtained from the finite element method (Tables (3a) and (3b)). Using Eqs. (61) and (62), we can calculate the natural frequency of the coupled system for any h_f if we have the value of one natural frequency of the fluid–membrane system for known h_f. This is the main advantage of the proposed approximate formulation. It should be noted that the relative error in Tables (3a) and (3b) is less that 2.5%. It is clear from these tables that there is a good agreement between the results obtained by approximate formula and those obtained by using the finite element method.

7. Concluding remarks

Two-dimensional coupled free vibrations of a fluid-filled rectangular container with a sagged bottom membrane were analyzed in this paper. The membrane material was assumed to be inextensible, and its weight was neglected in the computation of the equilibrium state. The container was filled with an incompressible and inviscid fluid. To facilitate the use of a two-dimensional analysis, the system was assumed to be extremely long and straight.

The governing equations for small vibrations about the equilibrium configuration were formulated. The equilibrium shape of the fluid–membrane system was obtained by using the analytical method proposed in this paper. The small vibration of the system was solved using the finite element method. The lowest six frequencies and corresponding mode shapes were also computed. Moreover, the variations of the natural frequencies with the pressure head, the membrane length, the membrane weight and the distance between two rigid walls were examined. The results showed that, in general, the natural frequencies of the fluid–membrane system increase as the membrane weight and the membrane length decrease, and as the pressure head increases. At the end of the analysis, we also proposed an approximate formula to determine the natural frequency of the coupled fluid–membrane system as a function of the pressure head.

Acknowledgments

The authors would like to sincerely thank Professor Padoussis for his comments and suggestions. We also thank the anonymous reviewers for their valuable comments on the manuscript.

Appendix A. Derivation of dynamic curvature

We introduce the following notation: $\overline{\mathbf{x}} = \mathbf{x_e} + \mathbf{y}$ and $\mathbf{y} = v_t^d\mathbf{t} - v_n^d\mathbf{n}$, that is, v_t^d and v_n^d are the tangential and normal perturbations. Assuming the normal to the boundary is pointing outwards, we can derive the following relations:

$$\frac{\partial\overline{\mathbf{x}}}{\partial s} = \frac{\partial\mathbf{x_e}}{\partial s} + \frac{\partial\mathbf{y}}{\partial s} = \left(1 + \frac{\partial v_t^d}{\partial s} - \kappa v_n^d\right)\mathbf{t} - \left(\frac{\partial v_n^d}{\partial s} + \kappa v_t^d\right)\mathbf{n}, \tag{A.1}$$

$$\frac{\partial^2\overline{\mathbf{x}}}{\partial s^2} = \frac{\partial^2\mathbf{x_e}}{\partial s^2} + \frac{\partial^2\mathbf{y}}{\partial s^2} = \left(\frac{\partial^2 v_t^d}{\partial s^2} - \frac{\partial\kappa}{\partial s}v_n^d - 2\kappa\frac{\partial v_n^d}{\partial s} - \kappa^2 v_t^d\right)\mathbf{t} - \left(\kappa + 2\kappa\frac{\partial v_t^d}{\partial s} - \kappa^2 v_n^d + \frac{\partial\kappa}{\partial s}v_t^d + \frac{\partial^2 v_n^d}{\partial s^2}\right)\mathbf{n}. \tag{A.2}$$

It should be noted that the following relations is used in derivation of the Eqs. (A.1) and (A.2)

$$\frac{\partial \mathbf{t}}{\partial s} = -\kappa \mathbf{n}, \quad \frac{\partial \mathbf{n}}{\partial s} = \kappa \mathbf{t}, \quad \kappa = \frac{\partial \psi_s}{\partial s}. \tag{A.3}$$

The curvature of the membrane in instantaneous deformed boundary ($\overline{\kappa} = \partial\psi/\partial s$) is given by

$$\overline{\kappa} = \frac{\frac{\partial^2 \overline{\mathbf{x}}}{\partial s^2} \cdot \mathbf{n}}{\frac{\partial \overline{\mathbf{x}}}{\partial s} \cdot \frac{\partial \overline{\mathbf{x}}}{\partial s}}. \tag{A.4}$$

Substituting Eqs. (A.1) and (A.2) into Eq. (A.4) and neglecting the higher order terms in v_t^d and v_n^d, the dynamic curvature is obtained as

$$\overline{\kappa} = \kappa + \frac{\frac{\partial^2 v_n^d}{\partial s^2} + \kappa^2 v_n^d + \frac{\partial \kappa}{\partial s} v_t^d}{1 + \frac{\partial v_t^d}{\partial s} - \kappa v_n^d}, \tag{A.5}$$

or

$$\frac{\partial \psi}{\partial s} = \frac{\partial \psi_s}{\partial s} + \frac{\frac{\partial^2 v_n^d}{\partial s^2} + \left(\frac{\partial \psi_s}{\partial s}\right)^2 v_n^d + \frac{\partial^2 \psi_s}{\partial s^2} v_t^d}{1 + \frac{\partial v_t^d}{\partial s} - \frac{\partial \psi_s}{\partial s} v_n^d} = \mathfrak{A} + \frac{\frac{\partial^2 v_n^d}{\partial s^2} + \mathfrak{A}^2 v_n^d + \mathfrak{B} v_t^d}{1 + \frac{\partial v_t^d}{\partial s} - \mathfrak{A} v_n^d}. \tag{A.6}$$

The difference between ψ and ψ_s can be seen in Eq. (A.6).

References

Amabili, M., Padoussis, M.P., Lakis, A.A., 1998. Vibrations of partially filled cylindrical tanks with ring-stiffeners and flexible bottom. Journal of Sound and Vibration 213, 259–299.

Bathe, K.J., 1995. Finite Element Procedures. Prentice-Hall, Englewood Cliffs, New Jersey.

Bedford, A., Fowler, W., 1999. Engineering Mechanics: Dynamics, second ed. Addison-Wesley, Berkeley, CA.

Bermudez, A., Rodriguez, R., 1994. Finite element computation of the vibration modes of a fluid–solid system. Computer Methods in Applied Mechanics and Engineering 119, 355–370.

Bermudez, A., Duran, R., Rodriguez, R., 1997. Finite element solution of incompressible fluid-structure vibration problems. International Journal for Numerical Methods in Engineering 40, 1435–1448.

Biswal, K.C., Bhattacharyya, S.K., Sinha, P.K., 2004. Dynamic response analysis of a liquid-filled cylindrical tank with annular baffle. Journal of Sound and Vibration 274, 13–37.

Cheung, Y.K., Zhou, D., 2000. Coupled vibratory characteristics of a rectangular container bottom plate. Journal of Fluids and Structures 14, 339–357.

Chiba, M., Watanabe, H., Bauer, H.F., 2002. Hydroelastic coupled vibrations in a cylindrical container with a membrane bottom, containing liquid with surface tension. Journal of Sound and Vibration 251 (4), 717–740.

Chiba, M., 1994. Axisymmetric free hydroelastic vibration of a flexural bottom plate in a cylindrical tank supported on an elastic foundation. Journal of Sound and Vibration 169, 387–394.

Daneshmand, F., Sharan, S.K., Kadivar, M.H., 2004. Dynamic analysis of a gate–fluid system. ASCE Journal of Engineering Mechanics 130, 1458–1466.

Ghavanloo, E., Daneshmand, F., 2009. A semi-analytical approach for the nonlinear two-dimensional analysis of fluid-filled thin-walled pliable membrane tubes. European Journal of Mechanics A/Solids 28, 626–637.

Jeong, K.H., 2006. Hydroelastic vibration of two annular plates coupled with a bounded compressible fluid. Journal of Fluids and Structures 22, 1079–1096.

Karagiozis, K.N., Amabili, M., Padoussis, M.P., Misra, A.K., 2005. Nonlinear vibrations of fluid-filled clamped circular cylindrical shells. Journal of Fluids and Structures 21, 579–595.

Kelkar, V.S., Sewell, R.T., 1987. Fundamentals of the Analysis and Design of Shell Structures. Prentice-Hall, Inc, New Jersey.

Liang, C.C., Tai, Y.S., 2006. Shock responses of a surface ship subjected to noncontact underwater explosions. Ocean Engineering 33, 748–772.

Phadke, A.C., Cheung, K.F., 2003. Nonlinear response of fluid-filled membrane in gravity waves. ASCE Journal of Engineering Mechanics 129 (7), 739–750.

Padoussis, M.P., Luu, T.P., Prabhakar, S., 2008. Dynamics of a long tubular cantilever conveying fluid downwards, which then flows upwards around the cantilever as a confined annular flow. Journal of Fluids and Structures 24, 111–128.

Tao, L., Molin, B., Scolan, Y.M., Thiagarajan, K., 2007. Spacing effects on hydrodynamics of heave plates on offshore structures. Journal of Fluids and Structures 23, 1119–1136.

Wang, X., Bathe, K.J., 1997. Displacement/pressure based mixed finite element formulation for acoustic fluid–structure interaction. International Journal for Numerical Methods in Engineering 40, 2001–2017.

Yuanjun, H., Xingrui, M., Pingping, W., Benli, W., 2007. Low-gravity liquid nonlinear sloshing analysis in a tank under pitching excitation. Journal of Sound and Vibration 299, 164–177.